 CMES, vol.4, no.3&4, pp.365-380, 2003

Numerical modeling of shape-memory alloys in orthodontics

F. Auricchio[1] **L. Petrini**[2] **R. Pietrabissa**[3] **and E. Sacco**[4]

Abstract: Since 80's many devices were developed to exploit the unique blend of mechanical and biocompatibility properties of *shape memory alloys* in orthodontic applications. It results in a high clinical effectiveness, but also in a spreading of technical knowledge on the properties of the single appliances. The goal of the present contribution is to contrast this sense of bewilderness and to prepare the basis for a simulation tool able to support the orthodontist choice. In particular a finite-element beam with a one-dimensional constitutive law, able to describe the SMA superelasticity and shape memory effect, is presented: it is shown how computer modeling can be helpful in the understanding of the single appliance response as well as in the design of new more advanced, and possibly more effective, applications.

keyword: Shape memory alloys, orthodontics application, numerical simulations.

1 Introduction

Advances in production technologies and developments of new alloys as well as their progressive transfer from research to applications are producing a significant evolution in orthodontics.

In particular, while stainless steel and chrome-cobalt-nickel have been traditionally among the most popular alloys in clinical orthodontic practice, nickel-titanium (Ni-Ti) is registering an increasing use since the last two decades [Drake, Wayne, Powers, and Asgar (1982); Miura, Mogi, Ohura, and Hamanaka (1986); Sachdeva and Miyazaki (1990)]. In fact, due to a unique blend of mechanical and biocompatibility properties [Shabalovskaya (1996); Ryhanen (1999)], Ni-Ti or more generally *shape-memory alloys* (SMA) result in a high clinical effectiveness, often combined with a reduction in treatment duration and chairside time [Duerig, Pelton, and Stökel (1996); Gil and Planell (1998); Van Humbeeck, Stalmans, and Besselink (1998); Torrisi (1999); Chu, Dai, Zhu, and Mi (2000); Pelton, Stökel, and Duerig (2000)].

However, such a SMA technology transfer is resulting not only in new products – each one with its own geometrical and mechanical properties, hence in a wider spectrum of possible orthodontic treatments – but also in a spreading and dispersion of technical knowledge on the properties of the single appliances.

In fact, even limiting the discussion to SMA materials, the dental market is characterized by several producers, each one with a wide range of proposals. Accordingly, the orthodontist should be able to select the appliance with the geometry, the material and the mechanical properties which meet at best the demand for the specific clinical situation, and, due to all the available possibilities, the choice is becoming more and more complex. Moreover, the technical informations available on each single appliance are in general limited, making even more difficult for the practitioner to orient himself and to make the optimal choice.

This is particularly true since one of the SMA features consists in the fact that the material mechanical properties can be sensibly tuned through proper thermomechanical treatments. Accordingly, the effectiveness of each single appliance is closely related to the specific material properties.

The goal of the present contribution is to contrast this sense of bewilderness and to prepare the basis for a simulation tool able to support the orthodontist choice. To do so, after a brief review of the SMA mechanical behavior and their use in orthodontics, we show how com-

[1] Corresponding author. (auricchio@unipv.it, http://www.unipv.it/dms/auricchio) Dipartimento di Meccanica Strutturale, Università di Pavia, Via Ferrata 1, 27100 Pavia, Italy.

[2] Dipartimento di Meccanica Strutturale, Università di Pavia, Via Ferrata 1, 27100 Pavia, Italy.

[3] Laboratorio di Meccanica delle Strutture Biologiche, Dipartimento di Bioingegneria, Politecnico di Milano, P.zza Leonardo da Vinci 32, 20133 Milano, Italy

[4] Dipartimento di Meccanica, Strutture, A&T, Università di Cassino, Via Di Biasio 43, 03043 Cassino, Italy.

puter modeling can be helpful in the understanding of the single appliance response as well as in the design of new more advanced, and possibly more effective, applications.

2 Shape-memory materials

Shape-memory alloys (SMA) are "materials with an intrinsic ability to remember an initial configuration". This memory is revealed at the macroscopic level in two main unusual behaviors, the *superelastic effect* (SE) and the *shape-memory effect* (SME). In particular, the superelastic effect indicates the material ability to undergo large deformations – up to 10-15% strains – in mechanical loading-unloading cycles without showing permanent deformations; the shape-memory effect indicates the material ability to present inelastic deformations during mechanical loading-unloading cycles, which can be recovered through thermal cycles.

As usual, the macro-behavior finds its explanation and justification in the underlying micro-mechanics.

From a crystallographic point of view, shape-memory alloys may in general present two different structures, one characterized by a more ordered unit cell, the *austenite* (A), the other characterized by a less ordered unit cell the *martensite*. Moreover, the martensite may have a global structure where the unit cells have a variable orientation minimizing the misfit with the surrounding material, or a global structure where the unit cells follow a preferred orientation given by an external field such as stress; in the former case we talk of *twinned or multiple-variant martensite* (M), in the latter case of *detwinned or single-variant martensite* (S).

From a micro-mechanical point of view, the presence of two different crystallographic structures is the base for a reversible solid-solid phase transformation between the austenite and the martensite. The phase transformation is in general function of temperature and stress. In particular, for the case of a stress-free material, we may distinguish two reference temperatures, A_f and M_f, with $A_f > M_f$, such that: the austenite is the only phase stable at temperatures above A_f; the martensite is the only phase stable at temperatures below M_f; an austenite-martensite mixture is possible in the temperature interval between A_f and M_f. In general, both A_f and M_f depend on the material composition as well as on the thermo-mechanical treatment. For the case of a stressed material, a similar situation occurs, with the difference that the reference temperatures are monotonic (approximatively linear) function of the loading level.

From a macro-mechanical point of view, as mentioned above, the reversible martensitic phase transformation results in two unique effects, the *superelasticity* (SE) (or pseudoelasticity) and the *shape memory effect* (SME). At temperatures above A_f, if loaded the material shows non-linear large deformations, which are recovered during the unloading, describing an hysteretic loop in terms of stress and strain (Figure 1). This response can be explained noting that the load induces a transformation from austenite to single-variant martensite; however, since the austenite is the only phase stable above A_f, the reverse transformation occurs during the unloading. At temperatures below A_f, if loaded the material shows non-linear large deformations, which are partially retained during the unloading; however, this residual strain can be recovered heating the material above A_f (Figure 2). This response can be explained noting that the load induces a transformation from austenite or multiple-variant martensite to single-variant martensite and that both type of martensite are stable for temperature below A_f in the case of unstressed material. However, since the martensite is unstable above A_f, heating the material, a transformation from martensite to austenite occurs and the material recovers the initial shape; moreover, such a shape is retained also during the cooling at the initial temperature.

As a consequence of these two behaviors, in general not present in traditional materials, shape-memory alloys lend themselves to be used in innovative applications relative to many different fields, ranging from cardiovascular non-invasive surgery to micro-actuator for endoscopy, and in particular relative to orthodontics, as discussed in the following Section.

2.1 Applications in orthodontics

Dental movement during orthodontic therapy is achieved by applying forces to teeth, resulting in a bone remodeling process. The optimal tooth movement is in general achieved applying forces which are low in magnitude and continuous in time; in fact, light constant forces are optimal to induce physiological dental movements without damaging the underlying tissues as well as to minimize patient discomfort. In contrast, forces with high mag-

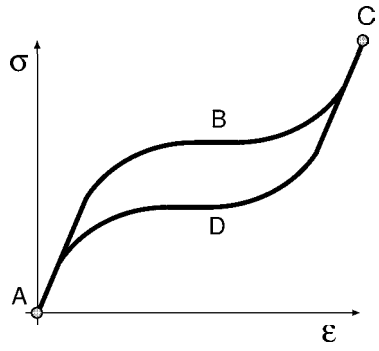

Figure 1 : Superelasticity effect. At a constant high temperature the material is able to undergo large deformations with zero final permanent strain.

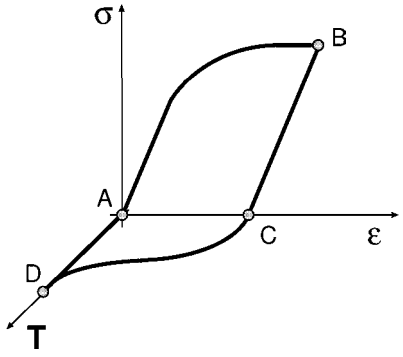

Figure 2 : Shape-memory effect. At the end of a mechanical loading-unloading path (*ABC*) performed at a constant low temperature, the material presents residual deformation (*AC*), which can be recovered through a thermal cycle (*CDA*).

nitude encourage hyalinization [5] of the periodontal ligament and they may cause irreversible tissue damage and root resorption.

Accordingly, SMA appliances, such as archwires or retraction loops, are more effective compared to appliances made of classical alloys, since they take advantage of the material ability to exert light constant springback forces over a large range of deformations [Duerig, Pelton, and Stökel (1996)]. Moreover, they are particularly suitable in situations requiring large deflections such as the preliminary alignment stage, in most cases resulting also in a limited mobility at the end of the therapy.

It is interesting to observe that a large variety of situations can occur, depending on the archwire geometrical parameters, on the material properties as well as on the specific loading conditions. Moreover, the oral cavity temperature varies during the day, for example due to the intake of cold or hot drink; henceforth, the springback force may also vary and it would important to control the variation range in terms of therapy effectiveness and patient comfort.

3 A SMA finite-element beam

In the present section, we briefly review the finite-element beam model proposed and discussed in Reference [Auricchio and Sacco (1999)]. The beam is able to describe the extension-bending response of a shape-memory element both in the superelastic and in the shape-memory range; accordingly, it is a valid computational tool for the simulation of orthodontic appliances, as shown in Section 4.

3.1 Superelastic and shape-memory constitutive model

The macroscopic material behavior is described through a one-dimensional constitutive model, cast within the *generalized plasticity theory* [Lubliner and Auricchio (1996)], adopting as control variables the uniaxial strain, ε, and the temperature, T. In the following we review the model basic ingredients.

Phase transitions and activation rules. We assume to describe the material crystallographic state through three scalar variables [6]:

- multiple-variant martensite fraction, ξ_M
- single-variant martensite fraction, ξ_S
- austenite fraction, ξ_A

[5] Hyalinization. Pathology: the forming of hyalin, a smooth, glassy substance resulting from some types of tissue and cell disintegration har (2001).

[6] By convention, the capital letters M, S and A used as subscripts refer to specific material fractions. Accordingly, $\xi_i = 0$ (with $i = M,S,A$) indicates absence of the corresponding phase, while $\xi_i = 1$ indicates that the material is completely in the indicated phase.

which should fulfill the following relation at any time: [7]

$$\xi_M + \xi_S + \xi_A = 1 \tag{1}$$

Consequently, only two fractions are independent, in the following chosen to be ξ_M and ξ_S [Auricchio and Lubliner (1997); Auricchio, Taylor, and Lubliner (1997)].

Experimental investigations show that for the adopted internal variables, in a uniaxial stress-temperature regime and in the usual range of applications, the region in which phase transformations may occur are delimited with good approximation by straight lines (Figure 3). Dealing with

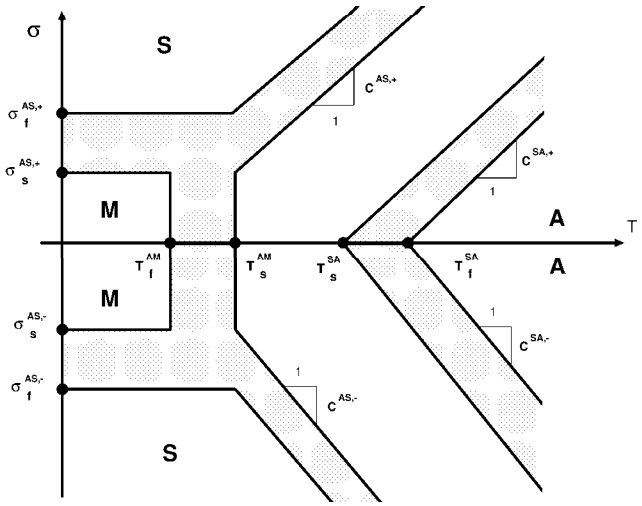

Figure 3 : Phase transformation zones in uniaxial tension and compression. Experimental investigations show that in a uniaxial stress-temperature diagram and in the usual range of applications the region in which phase transformations may occur (indicated in the figure with a dotted pattern) are delimited with good approximation by straight lines. We also indicates the regions in which only single fractions are stable (S: single-variant martensite, M: multiple-variant martensite, A: austenite).

three material fractions, we consider the corresponding three production processes:

- *Production of multiple-variant martensite.* It can occur only as conversion (reduction) of austenite and the region for the phase transformation occurrence is expressed through the following material parameters [8]:
  - o T_s^{AM}, representing the temperature at which the transformation starts at zero stress
  - o T_f^{AM}, representing the temperature at which the transformation finishes at zero stress
- *Production of single-variant martensite.* It can occur at the expenses of the austenite as well as at the expenses of the multiple-variant martensite. Based on experimental evidences, the region for the phase transformation occurrence is piecewise linear in temperature and it expressed through the following material parameters:
  - o C^{AS}, representing the phase transformation Clausius-Clapeyron constant
  - o σ_s^{AS}, representing the stress value at which the transformation starts for temperature below T_s^{AM}
  - o σ_f^{AS}, representing the stress value at which the transformation finishes for temperature below T_s^{AM}
- *Production of austenite.* It can occur at the expenses of the multiple-variant martensite as well as at the expenses of the single-variant martensite. The region for the phase transformation occurrence is expressed through the following material parameters:
  - o C^{SA}, representing the phase transformation Clausis-Clapeyron constant
  - o T_s^{SA}, representing the temperature at which the transformation starts at zero stress
  - o T_f^{SA}, representing the temperature at which the transformation finishes at zero stress

Strain decomposition and martensite reorientation. We assume an additive decomposition of the strain between an elastic quota, a phase-transformation quota and a thermal-expansion quota. Recalling that only the single-variant martensite can give a contribution to the strain [Wayman (1964)], we set:

$$\varepsilon = \varepsilon^e + \xi_S \beta + \alpha(T - T_o) \tag{2}$$

[7] For simplicity the dependency of the variables on a scalar parameter, such as time, is not explicitly stated.

[8] By convention, the superscripts refer to specific evolution processes; as an example, the superscript *AM* refers to the conversion of austenite into multiple-variant martensite.

where ε^e is the elastic strain, α and T_o are material parameters with:

- o α, representing the thermal expansion coefficient
- o T_o, representing an initial reference temperature in which the material is unstrained, unstress and fully in the austenitic phase

while β is an internal variable describing the orientation of the martensite. In particular, being in a one-dimensional setting, β represents the change of martensite orientation corresponding to a change from tension to compression or viceversa.

Different models can be introduced to describe the reorientation process. As discussed in Reference [Auricchio and Sacco (1999)], we consider a simple mechanisms expressed through the following material parameters:

- o γ, measuring the velocity of the reorientation process
- o σ^{SS}, representing the stress threshold for the activation of the reorientation process

Moreover, the reorientation process is such that in the limit $\beta \to \varepsilon_L \mathrm{sgn}(\sigma)$, with the material parameter:

- o ε_L, representing the recoverable strain or maximum residual strain,

Accordingly, ε_L is a measure of the maximum deformation obtainable only by multiple-variant martensite detwinning, hence, a measure of the maximum deformation obtainable aligning all the single-variant martensites in one direction [Wayman (1964); Brinson (1993)].

Elastic relation. We choose a linear elastic stress-strain relation; taking into account Equation 2, we set:

$$\sigma = E\Big[\varepsilon - \xi_S\beta - \alpha(T - T_0)\Big] \tag{3}$$

with E the Young's modulus. Due to the experimentally observed difference between the austenite and the martensite elastic properties, we introduce a dependence of E on the martensite fraction. In particular, the following functional form is adopted:

$$E(\xi_S) = \frac{E_A E_S}{E_S + \xi_S(E_A - E_S)} \tag{4}$$

where E_A and E_S are respectively the austenite and the martensite elastic moduli [Auricchio and Sacco (1997a)].

Remark 3.1 Because of the general framework in which the model is developed [Lubliner and Auricchio (1996)], there is no limitation on the relative position of the phase-transition zones; hence, they may intersect or they may be disjoint, since neither case would be problematic.

Remark 3.2 Experimental evidences show that shape-memory materials behave quite differently in tension and compression [Orgéas and Favier (1998); Gall, Sehitoglu, Chumlyakov, and Kireeva (1999); Lim and McDowell (1999)]. Recalling that we are dealing with a one-dimensional constitutive model, to obtain this effect, it is sufficient to distinguish between a set of material parameters valid in tension (indicated in the following with a superscript $+$) and a set of material parameters valid in compression (indicated in the following with a superscript $-$).

Accordingly, we need to distinguish between tension and compression for the following parameters:

$$C^{AS,+}\ ,\quad C^{SA,+}\ ,\quad \sigma_s^{AS,+}\ ,\quad \sigma_f^{AS,+}\ ,\quad \varepsilon_L^{+}\ ,\quad \sigma^{SS,+}$$

$$C^{AS,-}\ ,\quad C^{SA,-}\ ,\quad \sigma_s^{AS,-}\ ,\quad \sigma_f^{AS,-}\ ,\quad \varepsilon_L^{-}\ ,\quad \sigma^{SS,-}$$

while the parameters:

$$E_A\ ,\quad E_S\ ,\quad T_s^{AM}\ ,\quad T_f^{AM}\ ,\quad T_s^{SA}\ ,\quad T_f^{SA}\ ,\quad \gamma$$

are assumed to be equal in tension and compression.

3.2 Time-discrete model and solution algorithm

From a computational standpoint we treat the non-linear material behavior as a *time-discrete strain-driven* problem. Accordingly, as discussed in Reference [Auricchio and Sacco (1999)] we first introduce a time-discrete counterpart of the constitutive model and then compute the stress from the strain history by means of a *return-map* algorithm.

Time-discrete model. The time-discrete model is obtained integrating over the time interval $[t_n, t_{n+1}]$ the model rate equations, where t_n and t_{n+1} are two generic instant of time, such that $t_{n+1} > t_n$. In particular, we adopt a backward Euler scheme to integrate the equations.

Return-map algorithm. The corresponding time-discrete nonlinear problem is solved using a return-map

algorithm. The solution at time t_n is assumed to be known, together with the strain ε at time t_{n+1}.

The return-map is, in general, a two-step procedure of the type elastic-predictor inelastic-corrector, used for the integration of elastoplastic constitutive equations [Simo (1999)]. However, due to the specific model now investigated, a classical two-step return-map is not adequate as solution scheme. In fact:

- the evolutionary processes here considered are phase transformations; accordingly, for each of them there exist conditions at which the evolution is completed (exhausted). This results in a non-connected elastic domain [Lubliner and Auricchio (1996)].
- multiple phase transformations may be active at the same time

The details of the modified return-map algorithm can be found in Reference [Auricchio and Sacco (1999)], together with the algorithmically tangent moduli, obtained linearizing the stress constitutive equation in terms of the strain.

3.3 Finite-element beam

At this stage it is possible to develop a finite-element formulation for a beam made of a shape-memory material, whose constitutive behavior is described through the model presented in the previous Section.

A classical small-deformation Euler-Bernoulli beam theory is herein adopted [Popov (1990)]. The beam occupies a volume V, has cross-section A and length L. We indicate with (x,y,z) a Cartesian coordinate system having the x-axis coincident with the centerline axis of the undeformed beam. The x-y plane is also a plane of symmetry for the problem, such that the beam can undergo only elongation and deflection within this plane.

Kinematics and temperature field. Following the Euler-Bernoulli beam theory, the cross-sections are assumed to remain plain and orthogonal to the centerline of the deformed beam. The beam kinematics and deformation are defined as:

$$\begin{array}{lcll} u & = & u_o(x) - y v_o'(x) & \textit{axial displacement} \\ v & = & v_o(x) & \textit{transv. displacement} \\ \varepsilon & = & \varepsilon_o - y\chi & \textit{strain} \end{array} \tag{5}$$

where a superscript $'$ indicates a derivative with respect to x, while $\varepsilon_o = u_o'$ and $\chi_o = v_o''$ are the elongation and the curvature, respectively.

Moreover, in the present work we assume to neglect the production of thermal energy associated to the material fraction evolutions. According to this position, we retain the temperature as a given field (control variable); in particular, recalling the symmetry condition on the x-y plane, the thermal field is set to be linear in the cross section with y and constant along the beam axis:

$$T = \frac{T_d - T_u}{h}\, y + \frac{T_d + T_u}{2} \tag{6}$$

where T_d and T_u are respectively the temperature at the beam bottom and top, while h is the beam height.

Equilibrium equations. The beam equilibrium equations are derived introducing the kinematical assumptions into the principle of virtual displacement $L_{ve} = L_{vi}$, where L_{ve} and L_{vi} are the external and the internal virtual works, respectively. In particular, using Equation 5 the internal virtual work reduces to:

$$L_{vi} = \int_V \sigma\, \delta\varepsilon\, dV = \int_L \left[N \delta\varepsilon_o + M \delta\chi \right]\, dx \tag{7}$$

where the axial force N and the bending moment M are defined as:

$$N = \int_A \sigma\, dA \qquad , \qquad M = -\int_A y\sigma\, dA \tag{8}$$

Written in residual form, Equations 8 can be considered as the cross-section equilibrium equations.

Finite-element interpolation. The finite-element formulation is performed introducing an approximation on the displacement fields (u,v). The axial displacement u is taken linear along the beam axis, while the transversal displacement v is interpolated by the classical Hermite shape functions as required by the Euler-Bernoulli beam theory.

Substitution of the interpolation functions in the principle of virtual work returns the finite-element beam equilibrium equations. These nonlinear equations are first written in residual form and then solved through a Newton algorithm [Luenberger (1984)]. For the development of the Newton algorithm the following steps are required [9]:

[9] The adopted Newton scheme consists of two nested loops: the

1. time integration of the local constitutive equations
2. solution algorithm for the time-discrete equations
3. determination of the algorithmically tangent moduli
4. evaluation of the line and area integrals

In particular, the integration along the beam axis is performed numerically by Gauss formulas; the integration over the cross-section is performed discretizing the cross-section in strip elements orthogonal to the y-axis and applying again Gauss formulas within each strip. This computational scheme allows to calculate the martensite fraction distribution within each cross section and along the beam axis; in this way the effects of phase transition on the shape of the loaded beam, particularly evident during bending test, are caught, as deeply described by Auricchio and Sacco (1997b) and experimentally tested by Berg (1995).

Moreover, extensive numerical simulations assessing the performances of the proposed procedure in studying structures made of shape-memory materials have been detailed in Reference [Auricchio and Sacco (1999)].

4 Orthodontic simulations

As previously commented, SMA superelastic elements are very effective for the correction of teeth malocclusions in orthodontics, allowing to obtain an optimal teeth movement as well as to control and drastically shorten the therapy [Sachdeva and Miyazaki (1990)].

However, the investigation of orthodontic appliances can be very intrigate, not only as a consequence of the geometric parameter randomness but also, for example, as a consequence of the frequent temperature modifications in the oral cavity, due to possible food/drink intakes. These aspects lead to complex loading patterns and, in general, to a variable range for the recovery forces acting on the tooth, with possible consequent painful sensations as well as with an influence on the therapy effectiveness.

According to these considerations, the role of numerical simulations can be of non-negligible interest, as shown in the following. Herein, we focus on three different SMA orthodontic applications:

- archwire
- retraction T-loop
- retraction V-loop

For each problem we assume to start the simulation from an initial temperature T_0 (with $T_0 = 37\,^{\circ}\mathrm{C}$), corresponding to an unstrained, unstressed and fully austenitic state. Moreover, we study the appliance response under a mechanical loading followed by a thermal cyclic loading, the former attempting to reproduce the implantation procedure, the latter attempting to reproduce a possible food/drink intake.

The mechanical loading is imposed while keeping fixed the appliance temperature ($T = T_0 = 37\,^{\circ}\mathrm{C}$) and controlling the displacement d of some significative cross section; in particular, we distinguish between two different mechanical histories:

L: the displacement d of the significative cross section goes from zero up to a value d_{mec} (loading type history)

U: the displacement d of the significative cross section goes from zero up to a value d_{max} and then from the value d_{max} down to a value d_{mec}, with $d_{mec} < d_{max}$ (loading-unloading type history)

Moreover, the thermal loading is imposed while keeping fixed the displacement of the significative cross section ($d = d_{mec}$) and controlling the appliance temperature (T); in particular, we distinguish between two different thermal histories:

HC: the appliance temperature T goes from the initial value T_0 up to a value T_{max}, down to a value T_{min} and then back to the initial value T_0 (heating-cooling type history)

CH: the appliance temperature T goes from the initial value T_0 down to a value T_{min}, up to a value T_{max} and then back to the initial value T_0 (cooling-heating type history)

Accordingly, in the following we may have at most one of the following four possible loading combinations:

outer one relative to the satisfaction of the beam global equilibrium equations, the inner one relative to the satisfaction of the cross-section beam equations. For a more detailed discussion of the linearization and solution algorithm for the cross-section equilibrium equations, you may refer to Reference [Auricchio and Sacco (1997b)].

L-HC: mechanical loading followed by an heating-cooling thermal cycle

L-CH: mechanical loading followed by an cooling-heating thermal cycle

U-HC: mechanical loading-unloading followed by an heating-cooling thermal cycle

U-CH: mechanical loading-unloading followed by an cooling-heating thermal cycle

In the following, all the thermal cycles are characterized by the following temperature range:

$$T_{max} = 55\,^{o}\mathrm{C} \qquad T_{min} = 5\,^{o}\mathrm{C}$$

Finally, all the SMA elements considered are supposed to be made of a commercial Ni-Ti wire produced by GAC International Inc. This specific alloy has been experimentally investigated by Airoldi and coworkers in tensile and three-point bending conditions [Airoldi, Riva, and Vanelli (1995)]. Starting from their experimental results, we set for all the forthcoming investigations:

$$\begin{aligned}
E_A &= 55000 \text{ MPa} \\
E_S &= 25000 \text{ MPa} \\
\sigma_s^{AS,+} &= \sigma_f^{AS,+} = 130 \text{ MPa} \\
\sigma_s^{AS,-} &= \sigma_f^{AS,-} = 190 \text{ MPa} \\
\sigma^{SS,+} &= 30 \text{ MPa} \\
\sigma^{SS,-} &= 40 \text{ MPa} \\
C^{AS,+} &= 6 \text{ MPa}/^{o}\mathrm{C} \\
C^{SA,+} &= 9 \text{ MPa}/^{o}\mathrm{C} \\
C^{AS,-} &= 8.2 \text{ MPa}/^{o}\mathrm{C} \\
C^{SA,-} &= 11.4 \text{ MPa}/^{o}\mathrm{C} \\
T_s^{AM} &= 10\,^{o}\mathrm{C} \\
T_f^{AM} &= 5\,^{o}\mathrm{C} \\
T_s^{SA} &= T_f^{SA} = 25\,^{o}\mathrm{C} \\
\varepsilon_L^{+} &= 0.08 \\
\varepsilon_L^{-} &= 0.06 \\
\gamma &= 1 \text{ MPa/sec}
\end{aligned}$$

It is important to point out that the assessment of the constitutive-model material constants from the experimental data reported in Reference [Airoldi, Riva, and Vanelli (1995)] is a difficult and by no mean exhaustive process; in fact, the tests were originally not designed for this goal. Hence, even for the tensile case, the constants reported have some degree of discretionality; as an example, the choice of the recoverable strain ε_L^{+} is arbitrary and clearly it affects the global structural response investigated in the following.

Moreover, the uniaxial data available [Airoldi, Riva, and Vanelli (1995)] are all relative to tensile states. As a consequence, the determination of the constitutive-model constants for the compressive range are obtained in part extrapolating results relative to a Ni-Ti-Cu alloy [Adler, Yu, Pelton, Zadno, Duerig, and Barresi (1990); Auricchio, Taylor, and Lubliner (1997)].

4.1 Archwire

To investigate the response of a superelastic archwire, we first consider a simplifying case, i.e. a 3-point bending state, analyzing then the complete dental implant. It is interesting to observe that the 3-point bending situation has been often explored experimentally and some data are available in the literature; on the other hand, the study of the more realistic complete dental implant has always been neglected, possibly as a consequence of the problem greater complexity.

For both cases we consider a rectangular 0.558 mm (h) $\times$ 0.406 (b) mm cross-section.

3-point bending

Following the experimental investigations reported by Airoldi and coworkers [Airoldi, Riva, and Vanelli (1995)], we study the behavior of a simply supported beam subjected to a pointwise central force (three-point bending test) under the thermo-mechanical loading combination U-CH. In particular, the mechanical load is applied controlling the mid-span cross-section displacement with:

$$d_{max} = 8 \text{ mm} \qquad d_{mec} = 4 \text{ mm}$$

The beam has length $L = 14$ mm and, due to symmetry conditions, only half of the beam is discretized using a mesh of 30 elements with 4 Gauss points per element. The cross-section integrals are computed dividing each section in 20 strips and using 4 Gauss points in each strip.

As output parameter we consider the reaction force at the beam mid-span and Figure 4 shows the force variation in terms of deflection and temperature. It is interesting to observe how the numerical solution is able to reproduce the experimentally observed changes in the recovery force as a consequence of the intake of hot/cold quantities [Airoldi, Riva, and Vanelli (1995)], predicting a force on the teeth in the range of few newtons.

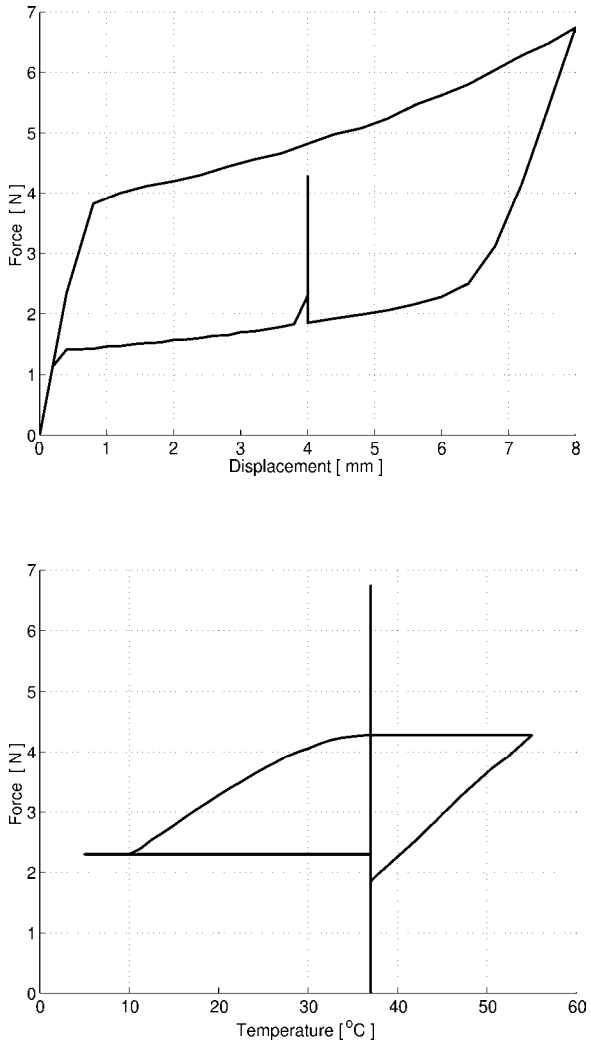

Figure 4 : Orthodontic wire. Applied force versus midspan deflection and temperature. The temperature cycle performed at fixed deflection ($d = 4.0$ mm) induces a change in the recovery force.

Complete implant

We now consider the complete archwire sketched in Figure 5. The geometrical parameters are:

$A = R = 30$ mm $\qquad B = 22.5$ mm

The mechanical load is applied controlling the displacement of a teeth (canine) in the direction orthogonal to the wire with:

$d_{max} = 8$ mm $\qquad d_{mec} = 4$ mm

The archwire is modeled using 5 beam elements between each couple of tooth. The interaction between the archwire and the single teeth is described with different boundary conditions (bc); in particular, we consider:

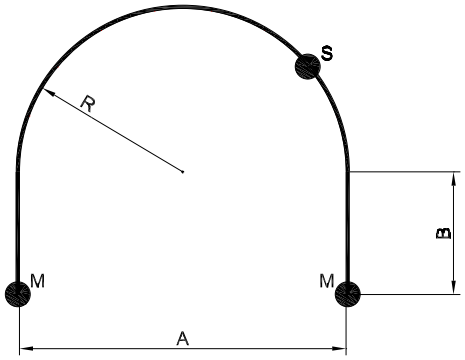

Figure 5 : Orthodontic archwire: geometric parameters.

- clamped or sliding roller for the molar teeth
- roller or hinge or sliding roller or clamped boundary conditions for the remaining teeth

Because the presented simulation tool is devoted to support the orthodontist choice, as output parameters we consider the reaction forces and moments on the canine (for which we control the displacement) and on the molar (closer to the former canine). In particular, we distinguish between force components orthogonal to the wire ($F_\perp$) and force components parallel to the wire ($F_\parallel$). Anyway, we remember the capability of the implemented model to calculate also other peculiar material behavior parameters, as the changes of the different phase volum fractions throughout the archwire during the mechanical loading [Auricchio and Sacco (1997b)].

Tables 1 and 2 reports the output parameters for all the thermo-mechanical loading and all the boundary conditions under investigations. It is interesting to observe that the only situation which predicts actions on the canine in the possible physiological range corresponds to sliding roller for all boundary conditions; this condition is also the one considered as the most consistent with effective practice.

As a final example, Figure 6 reports some deformed configuration at the end of the mechanical-thermal loading (U-CH) in comparison with the undeformed configuration (dotted line).

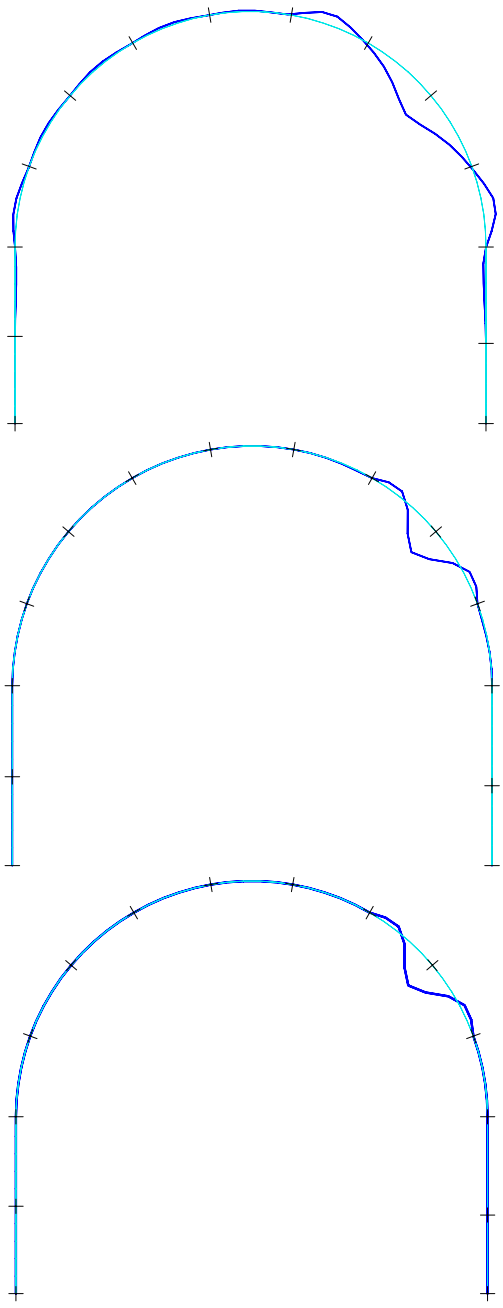

Figure 6 : Orthodontic archwire: Deformed configuration at the end of the mechanical-thermal loading (U-CH) and undeformed configuration (dotted line) for the following boundary conditions: clamped bc for the molar teeth and roller bc for the remaining teeth, clamped bc for the molar teeth and hinge bc for the remaining teeth, clamped bc for the molar teeth and clamped bc for the remaining teeth.

4.2 Retraction T-loop

We now investigate the response of a retraction appliance in the form of a T-loop, sketched in Figure 7. Following Reference [Raboud (1998)], the geometrical parameters are set equal to:

$A = 8$ mm $\quad B = 2$ mm $\quad C = 2.5$ mm
$D = 9$ mm $\quad R = 1$ mm

Moreover, we assume a rectangular 0.432 mm (h) $\times$ 0.635 mm (h) cross-section.

The appliance is mechanically loaded imposing outward displacements, equal in magnitude, on section S_c (Figure 7), assuming for the same sections no vertical displacements and no rotations (clamped boundary conditions). In particular, we set:

$d_{max} = 20$ mm $\quad d_{mec} = 10$ mm

As output parameters, we consider the horizontal reaction force and moment in section S_c; in general, we also report the moment/force ratio, since it represents the effective position of the applied force, hence a parameter of particular interest from the applicative perspective. The vertical reaction force is clearly equal to zero for symmetry reasons. Table 3 reports the output parameters for all the investigated thermo-mechanical loadings.

It is interesting to observe that:

- the force and the moment produced by the appliance varies in a quite small interval depending on the specific thermo-mechanical loading considered; however, all the values obtained are contained within the possible physiological range;
- the ratio moment/force produced by the appliance is almost constant independently from the specific thermo-mechanical loading considered.

Finally, we consider a parametric analysis for the T-loop rectraction appliance to investigate the effects induced by changes in the geometric parameters. The parametric analysis is expressed in terms of the following non-dimensional parameters:

$$A^\star = \frac{A}{A_0} \quad B^\star = \frac{B}{B_0} \quad C^\star = \frac{C}{C_0} \quad D^\star = \frac{D}{D_0} \quad R^\star = \frac{R}{R_0}$$

$$F_i^\star = \frac{F^i}{F_0^i} \quad M_i^\star = \frac{M^i}{M_0^i} \quad F_f^\star = \frac{F^f}{F_0^f} \quad M_f^\star = \frac{M^f}{M_0^f}$$

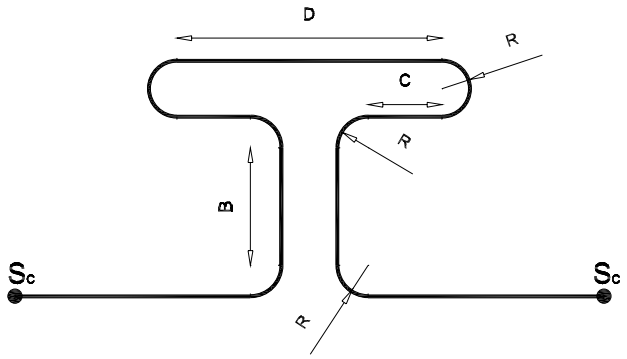

Figure 7 : T-loop retraction appliance: geometric data.

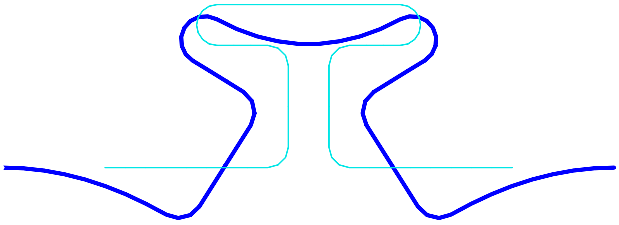

Figure 8 : T-loop retraction appliance: deformed configuration at the end of the mechanical-thermal loading (U-CH) and undeformed configuration (dotted line).

where the subscript 0 indicated the geometric and the output parameters relative to the appliance so far considered and in the following referred as "standard appliance". Accordingly, for the case of the "standard appliance" all the geometric and output non-dimensional parameters are equal to 1.

Table 4 reports the results relative to output parameters at the end of the thermo-mechanical loadings U-CH and U-HC, where we vary single geometric parameters.

It is interesting to observe:

- the geometric parameter $A^\star$, $C^\star$ and $D^\star$ have a small influence on the appliance response
- the geometric parameters $B^\star$ and $R^\star$ have a greater influence on the appliance response; in fact, increasing B and R increases the appliance flexibility, in particular, reducing only the horizontal stiffness (i.e. decreasing the horizontal force while keeping almost constant the moment), hence resulting in an increase of ratio moment/force

4.3 Retraction V-loop

We now investigate the response of a retraction appliance in the form of a V-loop, sketched in Figure 9. Following Reference [Raboud (1998)], the geometrical parameters are set equal to:

$$A = 8 \text{ mm} \qquad B = 4 \text{ mm} \qquad R = 1 \text{ mm}$$

Moreover, we assume the same rectangular cross-section as for the T-loop.

The appliance is mechanically loaded imposing outward displacements, equal in magnitude, on section S_c (Figure 9), assuming for the same sections no vertical displacements and no rotations (clamped boundary conditions). In particular, we set:

$$d_{max} = 20 \text{ mm} \qquad d_{mec} = 10 \text{ mm}$$

As output parameters, we consider the horizontal reaction force and moment in section S_c; in general, we also report the moment/force ratio, since it represents the effective position of the applied force, hence a parameter of particular interest from the applicative perspective. The vertical reaction force is clearly equal to zero for symmetry reasons. Table 5 reports the output parameters for all the investigated thermo-mechanical loadings.

It is interesting to observe:

- the force and the moment produced by the appliance varies in a quite small interval depending on the specific thermo-mechanical loading considered; however, all the values obtained are contained within the possible physiological range;
- the ratio moment/force produced by the appliance is almost constant independently from the specific thermo-mechanical loading considered.

Finally, we consider a parametric analysis for the V-loop rectraction appliance to investigate the effects induced by changes in the geometric parameters. The parametric analysis is expressed in terms of the following non-dimensional parameters:

$$A^\star = \frac{A}{A_0} \qquad B^\star = \frac{B}{B_0} \qquad R^\star = \frac{R}{R_0}$$

$$F_i^\star = \frac{F^i}{F_0^i} \qquad M_i^\star = \frac{M^i}{M_0^i} \qquad F_f^\star = \frac{F^f}{F_0^f} \qquad M_f^\star = \frac{M^f}{M_0^f}$$

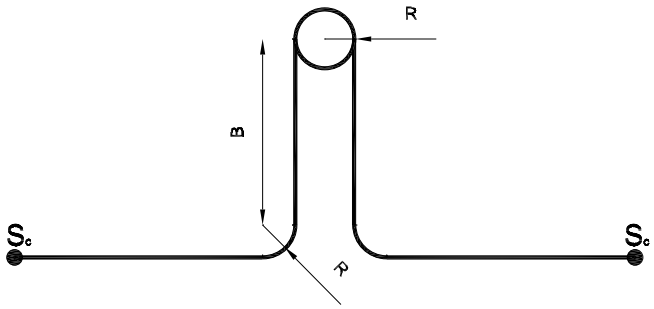

Figure 9 : V-loop retraction appliance: geometric data.

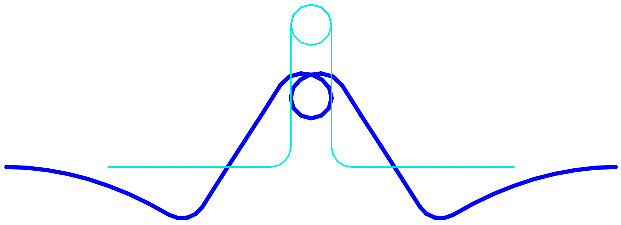

Figure 10 : V-loop retraction appliance: deformed configuration at the end of the mechanical-thermal loading (U-CH) and undeformed configuration (dotted line).

where the subscript 0 indicated the geometric and the output parameters relative to the appliance so far considered and in the following referred as "standard appliance". Accordingly, for the case of the "standard appliance" all the geometric and output non-dimensional parameters are equal to 1. Table 6 reports the results relative to output parameters at the end of the thermo-mechanical loadings U-CH and U-HC, where we vary single geometric parameters. It is interesting to observe:

- the geometric parameter $A^\star$ has a small influence on the appliance response
- the geometric parameters $B^\star$ and $R^\star$ have a greater influence on the appliance response; in fact, increasing B and R increases the appliance flexibility, in particular, reducing only the horizontal stiffness (i.e. decreasing the horizontal force while keeping almost constant the moment), hence resulting in an increase of ratio moment/force

Acknowledgement: The present work has been partially developed within the *Lagrange laboratory* French-Italian project as well as partially supported by the Italian National Center of Research (C.N.R) through the *Second Special Project for Advanced Technologies* ("Materiali Speciali per Tecnologie Avanzate II").

We wish to acknowledge Emiliano Miotti for helping in the literature search as well as in the numerical simulations.

References

Adler, P.; Yu, W.; Pelton, A.; Zadno, R.; Duerig, T.; Barresi, R. (1990): On the tensile and torsional properties of pseudoelastic Ni-Ti. *Scripta Metallurgica et Materialia*, vol. 24, pp. 943–947.

Airoldi, G.; Riva, G.; Vanelli, M. (1995): Superelasticity and shape-memory effect in Ni-Ti orthodontic wires. In *Proceedings of the International Conference on Martensitic Transformations (ICOMAT)*.

Auricchio, F.; Lubliner, J. (1997): A uniaxial model for shape-memory alloys. *International Journal of Solids and Structures*, vol. 34, pp. 3601–3618.

Auricchio, F.; Sacco, E. (1997): A one-dimensional model for superelastic shape-memory alloys with different elastic properties between austenite and martensite. *International Journal of Nonlinear Mechanics*, vol. 32, pp. 1101–1114.

Auricchio, F.; Sacco, E. (1997): A superelastic shape-memory-alloy beam model. *Journal of Intelligent Material Systems and Structures*, vol. 8, pp. 489–501.

Auricchio, F.; Sacco, E. (1999): A temperature-driven beam for shape-memory alloys: constitutive modelling, finite-element implementation and numerical simulations. *Computer Methods in Applied Mechanics and Engineering*, vol. 174, pp. 171–190.

Auricchio, F.; Taylor, R.; Lubliner, J. (1997): Shape-memory alloys: macromodelling and numerical simulations of the superelastic behavior. *Computer Methods in Applied Mechanics and Engineering*, vol. 146, pp. 281–312.

Berg, B. (1995): Bending of superelastic wires. Part I: Experimental aspects. *Journal of Applied Mechanics*, vol. 62, pp. 459–465.

Brinson, L. (1993): One-dimensional constitutive behavior of shape memory alloys: Thermomechanical derivation with non-constant material functions and redefined martensite internal variables. *Journal of Intelligent Material Systems and Structures*, vol. 4, pp. 229–242.

Chu, Y.; Dai, K.; Zhu, M.; Mi, X. (2000): Medical application of NiTi shape memory alloy in China. In *Proceedings of the International Sympos55-62ium on Shape Memory Materials, Materials Science Forum*, volume 327-328, pp. 55–62.

Drake, S.; Wayne, D.; Powers, J.; Asgar, K. (1982): Mechanical properties fo orthodontic wires in tension, bending and torsion. *American Journal of Orthodontics*, vol. 82, pp. 206–210.

Duerig, T.; Pelton, A.; Stökel, D. (1996): The utility of superelasticity in medicine. *Bio-Medical Materials and Engineering*, vol. 6, pp. 255–266.

Gall, K.; Sehitoglu, H.; Chumlyakov, Y.; Kireeva, I. (1999): Tension-compression asymmetry of the stress-strain response in aged single crystal and polycristalline NiTi. *Acta Materialia*, vol. 47, pp. 1203–1217.

Gil, F.; Planell, J. (1998): Shape memory alloys for medical applications. *Proceedings of the institution of mechanical engineers. Part H-Journal of Engineering in Medicine*, vol. 212 NH6, pp. 473–488.

Harcourt, Inc.. *Academic Press Dictionary of Science and Technology*, 2001. http://www.harcourt.com/dictionary/.

Lim, T.; McDowell, D. (1999): Mechanical behavior of an Ni-Ti alloy under axial-torsional proportional and non-proportional loading. *Journal of Engineering Materials and Technology*, vol. 121, pp. 9–18.

Lubliner, J.; Auricchio, F. (1996): Generalized plasticity and shape memory alloys. *International Journal Solids and Structures*, vol. 33, pp. 991–1003.

Luenberger, D. (1984): *Introduction to Linear and Nonlinear Programming*. Addson-Wesley Publishing Company.

Miura, F.; Mogi, M.; Ohura, Y.; Hamanaka, H. (1986): The super-elastic properties of the Japanese NiTi alloy wire for use in orthodontics. *American Journal of Orthodontics and Dentofacial Orthopedics*, vol. 90, pp. 1–10.

Orgéas, L.; Favier, D. (1998): Stress-induced martensitic transformation of NiTi alloy in isothermal shear, tension and compression. *Acta Materialia*, vol. 46, pp. 5579–5591.

Pelton, A.; Stökel, D.; Duerig, T. (2000): Medical use of Nitinol. In *Proceedings of the International Symposium on Shape Memory Materials, Materials Science Forum*, volume 327-328, pp. 63–70.

Popov, E. (1990): *Engineering Mechanics of Solids*. Prentice Hall.

Raboud, D. (1998): Simulation of the superelastic response of SMA orthodontic wires. *Journal of Biomechanical Engineering*, vol. 120, pp. 676–685.

Ryhanen, J. (1999): *Biocompatibility evaluation of nickel-titanium shape-memory metal alloy*. Ph.D. dissertation, University of Oulu, Department of Surgery, 1999.

Sachdeva, R.; Miyazaki, S. (1990): Superelastic Ni-Ti alloys in orthodontics. In Duerig, T.; Melton, K.; Stökel, D.; Wayman, C.(Eds): *Engineering aspects of shape memory alloys*, pp. 452–469.

Shabalovskaya, S. (1996): On the nature of the biocompatibility and on medical applications of Ni-Ti shape memory and superelastic alloys. *Bio-Medical Materials and Engineering*, vol. 6, pp. 267–289.

Simo, J. (1999): Topics on the numerical analysis and simulation of plasticity. In Ciarlet, P.; Lions, J.(Eds): *Handbook of numerical analysis*, volume III. Elsevier Science Publisher B.V.

Torrisi, L. (1999): The Ni-Ti superelastic alloy application to the dentistry field. *Bio-Medical Materials and Engineering*, vol. 9, pp. 39–47.

Van Humbeeck, J.; Stalmans, R.; Besselink, P. (1998): *Metals as Biomaterials*, chapter Shape memory alloys, pp. 73–100. Biomaterials Science and Engineering. John Wiley and Sons, 1998.

Wayman, C. (1964): *Introduction to the crystallography of martensitic transformations*. MacMillan.

Table 1 : Archwire: sliding roller boundary conditions for the molars. Appliance response on the canine for different thermo-mechanical loading histories and for different boundary conditions on the tooth (except the molars).

		$F^i_\perp$ [N]	$F^i_\parallel$ [N]	M^i [Nmm]	$F^f_\perp$ [N]	$F^f_\parallel$ [N]	M^f [Nmm]
Roller	L-HC	3.20	–	–	2.06	–	–
	L-CH	4.66	–	–	4.16	–	–
	U-HC	1.79	–	–	2.25	–	–
	U-HC	1.79	–	–	4.16	–	–
Hinge	L-HC	33.5	0.00	–	23.8	0.03	–
	L-CH	33.5	0.00	–	29.9	0.00	–
	U-HC	18.4	0.00	–	23.3	0.02	–
	U-CH	18.4	0.00	–	29.8	0.00	–
Sl.roller	L-HC	4.95	–	0.63	2.60	–	0.42
	L-CH	4.95	–	0.63	4.60	–	0.53
	U-HC	2.00	–	0.13	2.50	–	0.41
	U-CH	2.00	–	0.13	4.60	–	0.54
Clamped	L-HC	34.4	0.00	0.00	23.7	0.00	0.00
	L-CH	33.5	0.00	0.00	29.8	0.00	0.00
	U-HC	18.4	0.00	0.00	22.9	0.00	0.00
	U-CH	18.4	0.00	0.00	30.1	0.00	0.00

Table 2 : Archwire: clamped boundary conditions for the molars. Appliance response on a canine for different thermo-mechanical loading histories and for different boundary conditions on the tooth (except the molars).

		$F^i_\perp$ [N]	$F^i_\parallel$ [N]	M^i [Nmm]	$F^f_\perp$ [N]	$F^f_\parallel$ [N]	M^f [Nmm]
Roller	L-HC	17.7	–	–	10.4	–	–
	L-CH	17.7	–	–	14.8	–	–
	U-HC	6.88	–	–	10.2	–	–
	U-CH	6.88	–	–	14.8	–	–
Hinge	L-HC	33.5	0.00	–	23.8	0.03	0.00
	L-CH	33.5	0.00	–	29.9	0.00	–
	U-HC	18.4	0.00	–	23.3	0.02	–
	U-CH	18.4	0.00	0.00	29.8	0.00	–
Sl.roller	L-HC	20.9	–	0.67	12.5	–	0.67
	L-CH	20.9	–	0.67	17.7	–	0.60
	U-HC	11.1	–	1.73	12.2	–	0.68
	U-CH	11.1	–	1.74	18.1	–	0.38
Clamped	L-HC	34.4	0.00	0.00	23.7	0.00	0.00
	L-CH	33.5	0.00	0.00	29.8	0.00	0.00
	U-HC	18.4	0.00	0.00	22.9	0.00	0.00
	U-CH	18.4	0.00	0.00	30.1	0.00	0.00

Table 3 : Retraction T-loop: standard geometry. Appliance response for different thermo-mechanical loading histories.

	F_0^i [N]	M_0^i [Nmm]	F_0^f [N]	M_0^f [Nmm]	M_0^i/F_0^i [mm]	M_0^f/F_0^f [mm]
L-HC	3.19	9.48	1.53	4.57	2.97	2.99
U-HC	1.17	3.51	1.46	4.38	3.00	3.00
L-CH	3.19	9.48	2.85	8.50	2.97	2.98
U-CH	1.17	3.51	2.85	8.51	3.00	2.99

Table 4 : Retraction T-loop: parametric analysis for thermo-mechanical loading U-CH and U-HC.

$A^\star$ [-]	$B^\star$ [-]	$C^\star$ [-]	$D^\star$ [-]	$R^\star$ [-]	$F_i^\star$ [-]	$M_i^\star$ [-]	$F_f^\star$ [-]	$M_f^\star$ [-]	$M_i^\star/F_i^\star$ [-]	$M_f^\star/F_f^\star$ [-]
1.50	1	1	1	1	1.00	1.00	0.99	0.97	1.00	0.98
1	0.50	1	1	1	1.20	1.00	1.20	1.00	0.83	0.83
1	2	1	1	1	0.75	1.01	0.74	0.98	1.34	1.32
1	3	1	1	1	0.61	1.01	0.58	0.95	1.67	1.64
1	4	1	1	1	0.51	1.02	0.46	0.90	1.99	1.96
1	1	2	1.50	1	1.00	1.00	0.99	1.00	1.00	1.01
1	1	0	0.50	1	1.01	1.00	1.00	1.00	0.99	1.00
1	1	1	1.10	1.50	0.75	1.01	0.74	0.98	1.34	1.32
1	2	1	1.10	1.50	0.61	1.01	0.57	0.94	1.67	1.65
1.50	1	1	1	1	1.00	1.00	0.99	0.99	1.00	1.00
1	0.50	1	1	1	1.20	1.00	1.20	1.00	0.83	0.83
1	2	1	1	1	0.75	1.01	0.75	1.00	1.34	1.33
1	3	1	1	1	0.61	1.01	0.60	0.99	1.67	1.66
1	4	1	1	1	0.51	1.02	0.49	0.98	1.99	2.00
1	1	2	1.50	1	1.00	1.00	1.00	1.00	1.00	1.00
1	1	0	0.50	1	1.01	1.00	1.01	1.00	0.99	0.99
1	1	1	1.10	1.50	0.75	1.01	0.92	1.21	1.34	1.32
1	2	1	1.10	1.50	0.61	1.01	0.73	1.20	1.67	1.66

Table 5 : Retraction V-loop: standard geometry. Appliance response for different thermo-mechanical loading histories.

	F_0^i [N]	M_0^i [Nmm]	F_0^f [N]	M_0^f [Nmm]	M_0^i/F_0^i [mm]	M_0^f/F_0^f [mm]
L-HC	3.40	9.49	1.68	4.57	2.79	2.72
U-HC	1.30	3.50	1.60	4.37	2.69	2.73
L-CH	3.40	9.48	3.05	8.50	2.79	2.79
U-CH	1.30	3.50	3.05	8.50	3.05	2.79

Table 6 : Retraction V-loop: parametric analysis for thermo-mechanical loading U-CH and U-HC.

$A^\star$ [-]	$B^\star$ [-]	$R^\star$ [-]	$F_i^\star$ [-]	$M_i^\star$ [-]	$F_f^\star$ [-]	$M_f^\star$ [-]	$M_i^\star/F_i^\star$ [-]	$M_f^\star/F_f^\star$ [-]
1.50	1	1	1.00	1.00	0.99	0.97	1.00	0.98
0.50	1	1	1.00	1.00	1.01	1.03	1.00	1.02
1	0.50	1	1.88	0.99	1.77	1.00	0.53	0.57
1	1.50	1	0.70	1.01	0.72	0.98	1.44	1.36
1	2	1	0.55	1.01	0.55	0.95	1.83	1.71
1	2.50	1	0.46	1.02	0.45	0.90	2.21	2.01
1	1	1.50	0.82	1.00	0.82	0.99	1.23	1.21
1	1	2	0.68	1.01	0.70	0.98	1.47	1.39
1	1.50	2	0.55	1.01	0.55	0.94	1.83	1.72
1	2	2	0.46	1.02	0.45	0.90	2.22	2.02
1	2.00	3	0.40	1.03	0.35	0.83	2.59	2.37
1.5	1	1	1.00	1.00	1.19	1.21	1.00	1.01
0.5	1	1	1.00	1.00	1.01	1.00	1.00	1.00
1	0.5	1	1.88	0.99	1.83	0.99	0.53	0.54
1	1.5	1	0.70	1.01	0.71	1.00	1.44	1.40
1	2	1	0.55	1.01	0.56	1.00	1.83	1.77
1	2.5	1	0.46	1.02	0.46	0.99	2.22	2.16
1	1	1.5	0.82	1.01	0.83	1.00	1.23	1.20
1	1	2	0.68	1.01	0.69	1.00	1.47	1.44
1	1.5	2	0.55	1.02	0.56	0.99	1.84	1.79
1	2	2	0.46	1.03	0.46	0.98	2.22	2.13
1	2.00	3	0.40	1.04	0.39	0.97	2.59	2.50